A journal bearing with actively modified geometry for extending the parameter-based stability range of rotor-dynamic systems

Kai Becker[1]*, Wolfgang Seemann[2]

ISROMAC 2016

International Symposium on Transport Phenomena and Dynamics of Rotating Machinery

Hawaii, Honolulu

April 10-15, 2016

Abstract

The performance characteristics of a two-lobe journal bearing with an active adjustment of the bearing's geometry are analyzed. The fluid pressure is described by the Reynolds equation taking into account non-circular bearing geometries. The resulting fluid-film model is adapted to a two-lobe journal bearing which is later used in an elastic Jeffcott rotor.

In a first step the rotor system with time-constant geometry of the two-lobe bearings is investigated. By using solution continuation algorithms a higher rotational speed of stable equilibrium positions compared to a circular profile can be found.

Secondly the geometry of the bearings is varied harmonically during operation which results in additional pressure effects, such that self-excited oscillations can be suppressed or at least decreased in their amplitudes. The analysis is thereby carried out by means of Floquet-analysis for the special case of an unloaded rotor and afterwards transient simulations are used to examine the loaded system.

The numerical investigations proof that a higher admissible rotational speeds of an elastic rotor system can be reached, before instability phenomena such as "oil-whirl" and "oil-whip" occur.

Keywords

Reynolds equation, two-lobe bearing, Jeffcott rotor, Floquet analysis

[1] *Institute of Engineering Mechanics - Chair of Dynamics/Mechatronics, Karlsruhe Institute of Technology, Germany*

[2] *Institute of Engineering Mechanics - Chair of Dynamics/Mechatronics, Karlsruhe Institute of Technology, Germany*

*__Corresponding author__: kai.becker@kit.edu

INTRODUCTION

Fluid-solid interactions within journal bearings can lead to unwanted oscillations of the attached rotor system due to instabilities caused by non-linear effects. Depending on the bearing parameters and the angular velocity of the rotor, stable and unstable equilibrium points as well as limit-cycle behavior of the rotor system can be identified [1].

In order to reduce occurring oscillations and to extend the the stability range of the equilibrium positions, various methods have been proposed in literature. By using non-circular bearing geometries, the performance characteristics of rotor systems can be changed significantly, i.e. for static two-lobe or three-lobe bearings ([2], [3]). Furthermore various bearings with non-stationary geometries realized through displaceable elements are presented in literature. In the work of Chasalevris et al. [4], e.g. the influence of a variable geometry on the resonance behavior is analyzed using a passive adjustment through an appropriate spring-damper mechanism. In contrast to this the present work deals with an actively controlled bearing geometry in order to change the dynamic behavior of the corresponding rotor system operating at high rotational speeds. The relevant modeling assumption is based on a non-circular geometry, which is varied in the same scale like the actual fluid-film thickness. Therefore, the characteristic geometry of the bearing is not changed qualitatively, but additional pressure terms occur due to small changes of the geometry. The influence of these modifications can be significantly high, resulting in potential stabilization effects.

A general form of the Reynolds equation for non-stationary, non-circular bearing geometries is presented in section 1. Subsequently, an application on a two-lobe journal bearing is performed, which is characterized by its typical 'lemon-shaped' geometry. As a result the bearing support forces are presented based on a short bearing approach.

In section 3 the previously developed model of a two-lobe bearing is used for a Jeffcott rotor. Furthermore, the equations of motion are linearized around the trivial equilibrium position for the special case of an unloaded rotor.

Subsequently, a numerical analysis is carried out in section 4, focusing on a static two-lobe profile and afterwards on a time-varying profile.

Aiming for optimal geometry parameters of the profile, an analysis of the unloaded linearized system is performed in order to obtain a first educated guess for the non-linear loaded system.

A summary and discussion as well as an outline for possible further investigations can be found in section 5 .

1. REYNOLDS EQUATION FOR NON-CIRCULAR BEARING GEOMETRY

In the following section the Reynolds equation for a non-circular bearing geometry is presented. Starting with the geometric description, the fluid pressure differential equation

is derived as a modification of the classical Reynolds equation for circular profiles.

1.1 Geometry description

In the context of a variable non-circular but closed periodic bearing geometry, a general model with a variable radius distribution is assumed like depicted in figure 1.

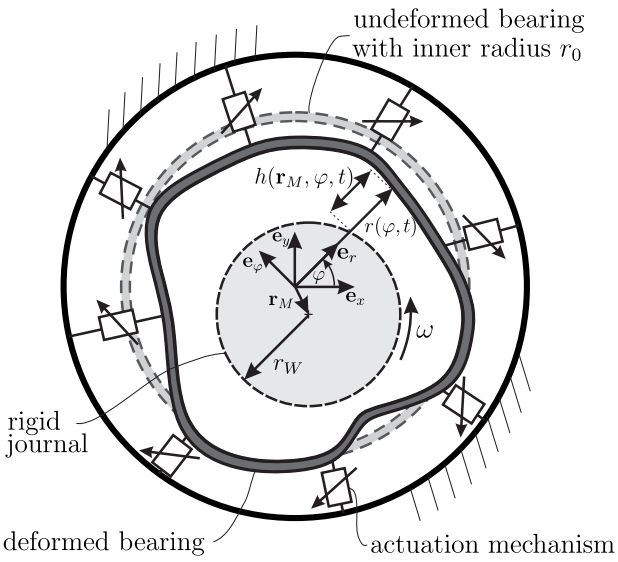

Figure 1. General non-circular bearing geometry

The bearing is supposed to be deformed by an actuation mechanism, which will not be considered in the following. The fluid-film-thickness is given by the function $h(\mathbf{r}_M, \varphi, t)$, which depends on the radius distribution as well as on the journal center coordinates $\mathbf{r}_M = x\mathbf{e}_x + y\mathbf{e}_y$ (cf. figure 1).
The resulting deformed geometry of the bearing is purely described by the radius $r(\varphi, t)$, which is considered to be just a function of the circumferential coordinate φ and time t. It is thereby assumed that the deviation from the undeformed circular shape

$$\Delta r(\varphi, t) = r(\varphi, t) - r_0 \tag{1}$$

is small compared to the radius r_0 of the undeformed profile. With the characteristic bearing clearance $C = r_0 - r_W$ a small scaling parameter can be defined

$$\varepsilon = \frac{r_0 - r_W}{r_0} = \frac{C}{r_0}, \tag{2}$$

which allows to state the necessary assumptions like the following:

$$\frac{h}{r_0} = O(\varepsilon), \quad \frac{\Delta r(\varphi, t)}{r_0} = O(\varepsilon). \tag{3}$$

Fluid-film thickness and radial deformation are therefore considered to be of the same scale, which is a necessary assumption for the following modeling of the pressure distribution within the fluid-film.

1.2 Reynolds equation

Due to the thin-film approach the pressure distribution in the bearing can be modeled by the Reynolds equation, expressed in polar coordinates for circular bearing profiles [5].
In this context the general non-dimensional form of the Reynolds equation is given by

$$\frac{\partial}{\partial\varphi}\left(\frac{\partial\Pi}{\partial\varphi}H^3\right) + \gamma^2\frac{\partial}{\partial\overline{z}}\left(\frac{\partial\Pi}{\partial\overline{z}}H^3\right) = 6\frac{\partial H}{\partial\varphi} + 12\frac{\partial H}{\partial\tau} \tag{4}$$

with the commonly used substitutions (cf. [5])

$$\overline{z} = \frac{2z}{B}, \quad H = \frac{h}{C}, \quad \Pi = \varepsilon^2\frac{p}{\mu\omega}, \quad \gamma^2 = \frac{4r_0^2}{B^2}, \quad \tau = \omega t. \tag{5}$$

In these relations the bearing's width along the axial coordinate z is denoted by B, the fluid pressure by p, the dynamic viscosity by μ. Furthermore, the dimensionless time τ is introduced, which is scaled according to the angular velocity ω of the rotating journal.
The non-dimensional pressure $\Pi(\varphi, \overline{z})$ is defined by the given partial differential equation (4), whereby the dimensionless fluid-film thickness reads out to be

$$H(X, Y, \varphi, \tau) = 1 + \overline{R}(\varphi, \tau) - X\cos\varphi - Y\sin\varphi. \tag{6}$$

The position of the journal's center with respect to the bearing's middle-point enters equation (6) via

$$X = \frac{x}{C} \quad \text{and} \quad Y = \frac{y}{C} \tag{7}$$

respectively.
The fluid-film thickness takes an additional term $\overline{R}(\varphi, \tau)$ into account, which results from the deviations from the circular profile (cf. equation (1)). Since the derivation of the Reynolds equation (4) is based on a power series approach [6], the function $\overline{R}(\varphi, \tau)$ can be obtained through a series expansion in ε of the shape deviation:

$$\frac{\Delta r}{C} = \frac{1}{C}(\varepsilon\Delta r_1 + \varepsilon^2\Delta r_2 + O(\varepsilon^3)) \tag{8}$$

$$\overline{R}(\varphi, \tau) = \frac{\varepsilon}{C}\Delta r_1(\varphi, \tau) \tag{9}$$

2. CHARACTERISTICS OF TWO-LOBE BEARING

Like depicted in figure 2 the two-lobe bearing is composed of two rigid cylindrical shells (lobes) of radius r_0, which are eccentrically arranged. This eccentricity is described by the vertical displacement function $d(t)$, which is assumed to be of same scale like the fluid-film thickness (cf. (3)). The displacement of upper and lower lobe is thereby considered to be symmetric.

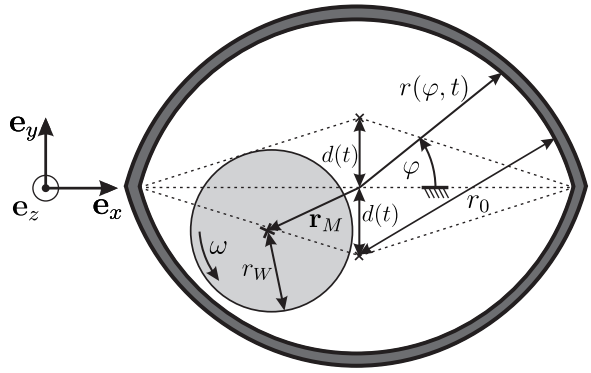

Figure 2. Geometry of two-lobe bearing

2.1 Two-lobe geometry

Setting up the correct expression of the bearing's geometry yields

$$r(\varphi,t) = \sqrt{r_0^2 - d(t)^2\,\cos^2\varphi}\; - d(t)\,|\sin\varphi| \tag{10}$$

within the circumferential range $\varphi \in [0, 2\pi)$.
Assuming $d(t)/r_0 = O(\varepsilon)$, the geometry function in (10) can be expressed as power series in terms of ε:

$$\frac{r(\varphi,t)}{r_0} = \underbrace{\frac{r_0}{r_0}}_{=O(1)} - \underbrace{\frac{d(t)}{r_0}|\sin\varphi|}_{=O(\varepsilon)} + O(\varepsilon^2)\,. \tag{11}$$

Considering only terms in the scale of $O(\varepsilon)$, the relevant term for describing the fluid-film thickness according to equation (9) is given by:

$$\overline{R}(\varphi,\tau) = -\frac{d(\tau)}{C}\,|\sin\varphi| = -D(\tau)\,|\sin\varphi| \tag{12}$$

This function is now used for determining the fluid-film thickness of the two-lobe bearing like given in equation (6).

2.2 Pressure distribution

The pressure distribution results from solving the Reynolds equation (4). In order to allow a first simple approach, the short bearing theory (SB) according to [7] is used by neglecting the partial derivatives with respect to the circumferential coordinate φ.
For the short bearing approach ($\gamma \gg 0 \Rightarrow \Pi \approx \Pi^{\mathrm{SB}}$) the partial differential equation (PDE) can be solved analytically for the pressure with the assumed axial boundary conditions $\Pi^{\mathrm{SB}}(\varphi, \overline{z} = \pm 1) = 0$:

$$\begin{aligned}\Pi^{\mathrm{SB}} &= \frac{3(1-\overline{z}^2)}{\gamma^2}\,G(\varphi) \qquad \text{with}\\ G(\varphi) &= \left[\frac{(X - 2D'(\tau)\,\mathrm{sgn}(\sin\varphi) - 2y')\sin\varphi}{((D(\tau)\,\mathrm{sgn}(\sin\varphi)+Y)\sin\varphi + X\cos\varphi - 1)^3}\right.\\ &\quad\left. - \frac{(D(\tau)\,\mathrm{sgn}(\sin\varphi)+Y+2X')\cos\varphi}{((D(\tau)\,\mathrm{sgn}(\sin\varphi)+Y)\sin\varphi + X\cos\varphi - 1)^3}\right].\end{aligned} \tag{13}$$

$(\,)' = \frac{\partial(\,)}{\partial\tau}$ denotes thereby the derivative with respect to τ.

It is revealed that additional pressure effects are caused by the time-dependent eccentricity $D(\tau)$ ans its derivative $D'(\tau)$ as both terms enter the pressure distribution in equation (13). So with increasing velocity of the geometry variation also the resulting pressure can be increased.

2.3 Bearing forces

Focusing on the determined pressure distribution in equation (13) the bearing's support reactions can be calculated via an area integration of the pressure distribution

$$\begin{aligned}F_x &= \iint_{A_p} -p(\varphi,z)\cos\varphi\; r_W\,\mathrm{d}\varphi\mathrm{d}z\,,\\ F_y &= \iint_{A_p} -p(\varphi,z)\sin\varphi\; r_W\,\mathrm{d}\varphi\mathrm{d}z\end{aligned} \tag{14}$$

with the given integration range of positive pressures

$$A_p = \left\{(\varphi,z):\ \varphi\in[0,2\pi),\ z\in\left[-\frac{B}{2},\frac{B}{2}\right] : p(\varphi,z)\geq 0\right\}.$$

Negative pressures are an artificial phenomena of the Reynolds equation. Therefore, their influence needs to be eliminated through an appropriate integration domain [7].
Using equation (13) and the forces from (14) leads to

$$\begin{aligned}\frac{F_x}{F_0} &= \frac{r_W r_0^2 \mu\omega B}{2F_0C^2\gamma^2}\left[-\int_{\Omega_\varphi} G(\varphi)\left(\int_{-1}^{1} F(\overline{z})\mathrm{d}\overline{z}\right)\cos\varphi\;\mathrm{d}\varphi\right]\\ &= \frac{B^3 r_W\mu}{8F_0C^2}\omega\underbrace{\int_{\Omega_\varphi} -4G(\varphi)\cos\varphi\mathrm{d}\varphi}_{=:f_x} = S_m f_x\,,\\ \frac{F_y}{F_0} &= \frac{r_W r_0^2 \mu\omega B}{2F_0C^2\gamma^2}\left[-\int_{\Omega_\varphi} G(\varphi)\left(\int_{-1}^{1} F(\overline{z})\mathrm{d}\overline{z}\right)\sin\varphi\;\mathrm{d}\varphi\right]\\ &= \frac{B^3 r_W\mu}{8F_0C^2}\omega\underbrace{\int_{\Omega_\varphi} -4G(\varphi)\sin\varphi\mathrm{d}\varphi}_{=:f_y} = S_m f_y\end{aligned} \tag{15}$$

with the modified Sommerfeld-number $S_m = \frac{B^3 r_W\mu\omega}{8F_0C^2}$ according to [5] and a characteristic force F_0 used for a dimensionless representation.

Due to the kinks in the geometry which come into play through the term $|\sin\varphi|$ in equation (12) the pressure field is discontinuous at $\varphi = 0$ and $\varphi = \pi$. Nevertheless the kink does not affect the pressure forces very much. Numerical simulations showed that a smoothing of the geometry at the critical points has a rather small influence on the circumferential integration of the pressure distribution.

The identification of the exact integration domain

$$\Omega_\varphi = \{\varphi \in [0, 2\pi) : G(\varphi) \geq 0\} \tag{16}$$

in equation (15) is rather complicated, so for numerical reasons the domain is set constant, while a regularization of $G(\varphi)$ is carried out. The integral terms in the force expressions in (15) can therefore be approximated by n Gauss points within the integration range $\varphi \in [0, 2\pi)$

$$\begin{aligned} f_x \approx \tilde{f}_x &= -4 \sum_{i=1}^{n} a_i \ \max\left(G(\varphi_i), 0\right) \cos\varphi_i \,, \\ f_y \approx \tilde{f}_y &= -4 \sum_{i=1}^{n} a_i \ \max\left(G(\varphi_i), 0\right) \sin\varphi_i \end{aligned} \tag{17}$$

with the corresponding weighting factors a_i (cf. [8]).

3. JEFFCOTT ROTOR MODEL

For the rotor itself the classical Jeffcott model [9] is used, assuming a rigid disc of mass m mounted on an elastic shaft with linear elasticity c_s, supported by two journal bearings. The rotor is considered to be perfectly balanced, such that only self-exciting phenomena are investigated.
The bearings are modeled as two-lobe bearings with their support forces according to (15) and (17), assuming the short bearing theory.
In order to be able to build up a first order system for numerical simulations, two masses Δm are assigned to the shaft at the bearings' positions respectively.
Furthermore, the rotor is exposed to a vertical acting external force F and to an external viscous damping with linear damping coefficient d_a.

3.1 Equations of motion

Based on the previous modeling the corresponding equations of motion are given by the dimensionless form

$$\begin{aligned} \overline{\omega}^2 X_R'' + \overline{d}_a \overline{\omega} X_R' + \frac{X_R - X_B}{\Gamma} &= 0 \,, \\ \overline{\omega}^2 Y_R'' + \overline{d}_a \overline{\omega} Y_R' + \frac{Y_R - Y_B}{\Gamma} + f &= 0 \,, \\ \eta\overline{\omega}^2 X_B'' + \frac{X_B - X_R}{\Gamma} - \sigma\overline{\omega} f_x(X_B, Y_B, X_B', Y_B', \tau) &= 0 \,, \\ \eta\overline{\omega}^2 Y_B'' + \frac{Y_B - Y_R}{\Gamma} - \sigma\overline{\omega} f_y(X_B, Y_B, X_B', Y_B', \tau) &= 0 \end{aligned} \tag{18}$$

whereby the following substitutions are used (cf. [1]):

$$\begin{aligned} X_{R/B} = \frac{x_{R/B}}{C}, \ Y_{R/B} = \frac{y_{R/B}}{C} \,, \\ \overline{\omega}^2 = \frac{mC}{F_0}\omega^2, \ \sigma = \frac{2S_m}{\overline{\omega}}, \ \eta = \frac{2\Delta m}{m} \,, \\ \Gamma = \frac{F_0}{c_s\, C}, \ \overline{d}_a = \sqrt{\frac{C}{mF_0}}\, d_a, \ f = \frac{F}{F_0} \,. \end{aligned} \tag{19}$$

In this context Γ represents the compliance of the supporting shaft, $\overline{d}_a$ characterizes the viscous damping and η describes the mass ratio of the disc and the masses allocated to the bearings' positions. σ describes a bearing parameter, which is independent of the rotational speed, while f gives the influence of the outer force F. The relevant rotational speed-parameter is given by $\overline{\omega}$ and is considered to be essential for the stability and bifurcation investigations.
The displacements of the shaft inside the bearings (index B) and of the disc (index R) are scaled by the characteristic bearing clearance C.
The support reactions are given by the approximated integrals according to (17).

The bearings should optimize the dynamic behavior during operation through an actively controlled change of their geometry. Therefore, in a first approach the geometry is varied over time by the eccentricity factor $D(\tau)$ assuming a harmonic excitation

$$D(\tau) = \widehat{D}(1 + \delta_D \cos(\Omega\tau)) \tag{20}$$

with mean value $\widehat{D}$ and a time-dependent cosine-part with frequency Ω and relative amplitude δ_D.

3.2 Linearized model for unloaded rotor

In order to perform suitable stability investigations, an appropriate linearization of the system has to be carried out, while aiming for an extension of the stability of an equilibrium position of the system in (18).
Due to the time-variant bearing geometry, the fluid-film-thickness changes, even if the whole system coordinates stay constant, which generally results in non-constant bearing forces for rest positions. Solving the equations in (18) for an equilibrium position is therefore rather complicated, i.e. the existence of such a solution has not been proved so far.
Nevertheless for the special case $f = 0$ of an unloaded rotor the problem becomes symmetric and an equilibrium point can be found. Introducing the state-vector $\underline{z}$, the trivial equilibrium position $\underline{z}_0 = (X_{R_0}, Y_{B_0}, X_{R_0}, Y_{B_0}) = (0, 0, 0, 0)$ with $\dot{\underline{z}}_0 = (0, 0, 0, 0)$ exists.

The main parts of the equations in (18) are already linear, so only the bearing forces f_x, f_y have to be linearized.
In order to avoid further approximation errors through the performed Gauss quadrature in (17), the exact bearing forces from (15) are linearized while the involved integrals can be solved analytically within the corresponding integration boundaries for the given equilibrium point.
Applying a Taylor-series expansion, the linearized forces for the trivial equilibrium position read out to be

$$\begin{aligned} f_x^{\text{lin}} &= f_x|_{\underline{z}_0} + \left.\frac{\partial f_x}{\partial \underline{z}}\right|_{\underline{z}_0} (\underline{z} - \underline{z}_0) \,, \\ f_y^{\text{lin}} &= f_y\big|_{\underline{z}_0} + \left.\frac{\partial f_y}{\partial \underline{z}}\right|_{\underline{z}_0} (\underline{z} - \underline{z}_0) \end{aligned} \tag{21}$$

with

$$
\begin{aligned}
f_x|_{\underline{z}_0} &= f_y\Big|_{\underline{z}_0} = 0,\\
\frac{\partial f_x}{\partial \underline{z}}\bigg|_{\underline{z}_0} &= -4\left(\int_0^{b_U} \frac{\partial G}{\partial \underline{z}}\bigg|_{\underline{z}_0} \cos\varphi \,\mathrm{d}\varphi + \int_\pi^{b_L} \frac{\partial G}{\partial \underline{z}}\bigg|_{\underline{z}_0} \cos\varphi \,\mathrm{d}\varphi\right),\\
\frac{\partial f_y}{\partial \underline{z}}\bigg|_{\underline{z}_0} &= -4\left(\int_0^{b_U} \frac{\partial G}{\partial \underline{z}}\bigg|_{\underline{z}_0} \sin\varphi \,\mathrm{d}\varphi + \int_\pi^{b_L} \frac{\partial G}{\partial \underline{z}}\bigg|_{\underline{z}_0} \sin\varphi \,\mathrm{d}\varphi\right)
\end{aligned}
\tag{22}
$$

and the corresponding integration boundaries for the upper lobe

$$b_U = \operatorname{atan2}(\widehat{D}(1+\delta_D\cos(\Omega\tau)),\ 2\widehat{D}\,\delta_D\sin(\Omega\tau)) \tag{23}$$

and for the lower lobe respectively

$$b_L = b_U + \pi. \tag{24}$$

The resulting linear system is characterized by a periodic stiffness and damping matrix, caused by the chosen variation of the bearing geometry through the eccentricity factor in equation (20).

4. SYSTEM ANALYSIS

The system's behavior is investigated based on the derived equations of motion in section 3.
The analysis is carried out numerically by means of solution continuation delivered by the Matlab-toolbox MATCONT [10] and standard Floquet-analysis [11].
MATCONT is thereby used for numerical investigations of equilibria as well as of periodic solutions of systems of ordinary differential equations. Appropriate algorithms are provided to detect these solutions, to characterize their stability and to continue them in dependence of a chosen parameter, such that a bifurcation analysis can be carried out.
In the following the dimensionless rotational speed $\overline{\omega}$ is chosen as relevant bifurcation parameter for the numerical evaluation by means of MATCONT.

First the system with static geometry ($\delta_D = 0$) is investigated for its stability of equilibrium positions as well as for the limit-cycle behavior in dependence of the relevant rotational speed and geometry-parameters.
Subsequently, the system with a dynamically varying bearing geometry is analyzed. Using the linearized equations for an unloaded rotor as first approach towards the dynamics of the system, transient numerical simulations are performed.

The overall aim is thereby to identify suitable parameter values for the bearing geometry and its variation, in order to extend the stability range of potential equilibrium points or at least to decrease the amplitudes of existing limit-cycles.

4.1 Static geometry

In a first step an analysis of the system with static two-lobe bearings is carried out. The eccentricity function is thereby considered to be constant

$$D(\tau) = \widehat{D} = \text{const.} \tag{25}$$

In order to examine the influence of the system's rotational speed on the stability properties, a bifurcation analysis is carried out with $\overline{\omega}$ being the relevant bifurcation parameter.

MATCONT delivers the equilibrium points of the system in dependence of the chosen bifurcation parameter $\overline{\omega}$. In order to show the qualitative behavior, the results for one specific parameter-set are depicted in figure 3.

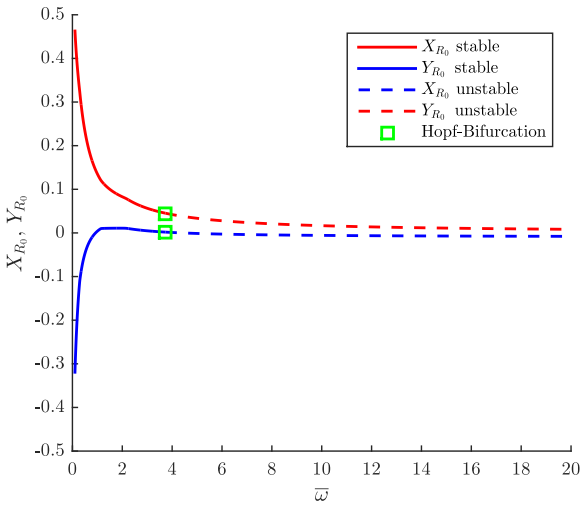

Figure 3. Equilibrium point of the rotor in dependence of $\overline{\omega}$ with $\widehat{D} = 0.1$, $\overline{d}_a = 0.1$, $\Gamma = 0.01$, $\eta = 0.25$, $\sigma = 1$, $f = 1$

With increasing rotation speed the equilibrium position of the rotor tends towards the bearing's center.
By reaching a critical value of $\overline{\omega}$, a Hopf-bifurcation leads to a loss of stability (represented by dashed line) of the equilibrium point and the creation of a stable limit-cycle. This behavior is often referred to as "oil-whirl" in literature [12] and can bee seen as typical for journal bearings.

In order to characterize the influence of the static eccentricity $\widehat{D}$ on the "oil-whirl" behavior, a continuation of the Hopf-bifurcation is performed in the $\widehat{D} - \overline{\omega}$−parameter-plane. In figure 4 the Hopf-bifurcation points are depicted for different compliance values of the shaft. It is revealed that the critical value of $\overline{\omega}$, at which the stability of the equilibrium point is lost, can be increased by enlarging the static eccentricity $\widehat{D}$. The positive effect of a decreasing compliance onto the critical value of $\overline{\omega}$ is in context with previous investigations in literature [9] and therefore reasonable; indeed the influence of the shaft's compliance seems to have a bigger effect when non-circular bearing profiles are used.

By increasing the rotational speed further than the critical value of the Hopf-bifurcation, limit-cycles occur. Figure 5

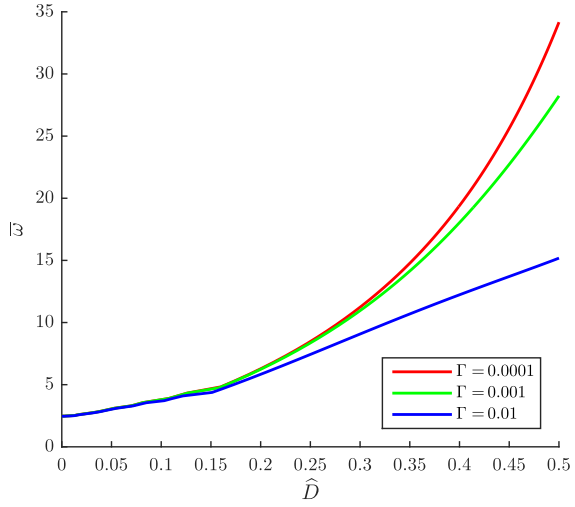

Figure 4. Hopf-bifurcation in $\widehat{D} - \overline{\omega}-$parameter-plane for different shaft compliance with $\overline{d}_a = 0.1$, $\eta = 0.25$, $\sigma = 1$, $f = 1$

shows the rotor's vertical amplitude in the super-critical rpm-range for different eccentricity factors.

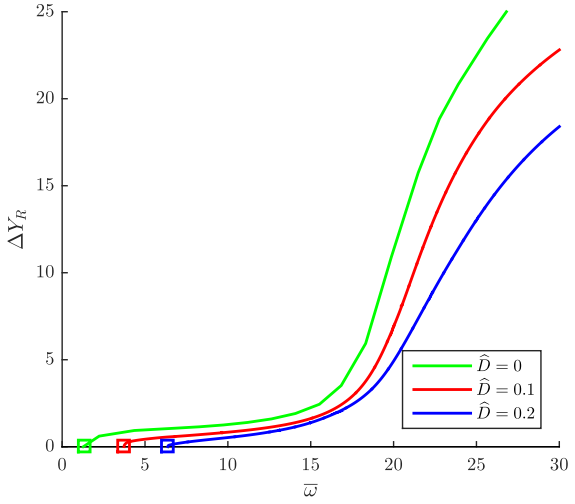

Figure 5. Limit-cycle amplitudes in vertical direction in dependence of $\overline{\omega}$ for different eccentricities $\widehat{D}$ with $\overline{d}_a = 0.1$, $\Gamma = 0.01$, $\eta = 0.25$, $\sigma = 1$, $f = 1$

Increasing the speed-parameter leads to a growing of the rotor's oscillation amplitude until a system's resonance frequency is reached, which results in a tremendous rise of the rotor amplitude, often referred to as "oil-whip" [13].
The effect of a non-circluar bearing profile becomes obvious. Compared to the circular profile at $\widehat{D} = 0$, the system with a two-lobe profile has a higher critical rotational speed, at which the limit-cycles start to evolve (cf. figure 4).
Apart from that, significantly lower rotor amplitudes are obtained at the same value of the speed-parameter compared to the system with circular bearing geometry, i.e. for a rotation speed in the "oil-whip" range of $\overline{\omega} = 25$ the vertical rotor amplitudes between the systems with an eccentricity of $\widehat{D} = 0$ and $\widehat{D} = 0.2$ differ by almost 40%.

4.2 Time-variant geometry

The system is now considered to be additionally excited via a changing bearing geometry. An eccentricity with harmonic time dependence is assumed according to equation (20) with a variation frequency Ω and relative amplitude δ_D. The system is thereby investigated in two steps.
First, the stability of the trivial equilibrium point of the unloaded system ($f = 0$) is investigated by analyzing the corresponding linearized equations, presented in section 3.2. For this purpose a Floquet-analysis is performed to determine stable and unstable regions in the $\overline{\omega} - \Omega-$parameter-plane and to detect the corresponding stability boundaries.
Based on the stable parameter-sets of the linearized model, transient numerical simulations of the original system with external load ($f \neq 0$) are carried out. Taking stable configurations of the unloaded problem as a first guess for suitable parameters of the loaded system seems reasonable, since it also approaches an environment around the trivial point with increasing rotational speed (cf. figure 3).

4.2.1 Analysis of the unloaded system

In comparison to the original non-linear equations the linearized ones can be simulated a lot faster and easier. In this context a stability analysis of the trivial equilibrium point of the unloaded system can be performed. Nevertheless, it is considered to be a sufficient basis for further parameter-studies of the loaded problem.
Due to the fact that time-dependent coefficients occur in the linearized equations, a regular Eigenvalue-analysis cannot be performed. Instead a Floquet-analysis [11] has to be carried out to determine the stability properties of the trivial solution. The aim is to achieve a stabilization of $\underline{z}_0$ for higher rotational speeds by introducing an appropriate frequency Ω.

A stability map in the $\overline{\omega} - \Omega-$parameter-plane is depicted in figure 6 for different values of the mean eccentricity $\widehat{D}$. The unstable regions are colored in gray while the depicted lines represent the stability boundaries. The white regions represent the parameter-sets for which asymptotic stability can be detected.
The characteristic 'nose'-shape in the lower speed range of both stability boundary curves is assumed to be in context with parametric resonance phenomena. Further investigations concerning this effect are in progress.

The stability of the trivial solution $\underline{z}_0 = (0, 0, 0, 0)$ is thereby lost through a Neimark-Sacker-bifurcation (cf. [14]). The numerical results show that the equilibrium point can be stabilized by an appropriate excitation frequency of the bearing's geometry. Therefore, self-excited vibrations of the unloaded rotor in higher rpm-ranges can be suppressed completely by creating an asymptotically stable equilibrium point.

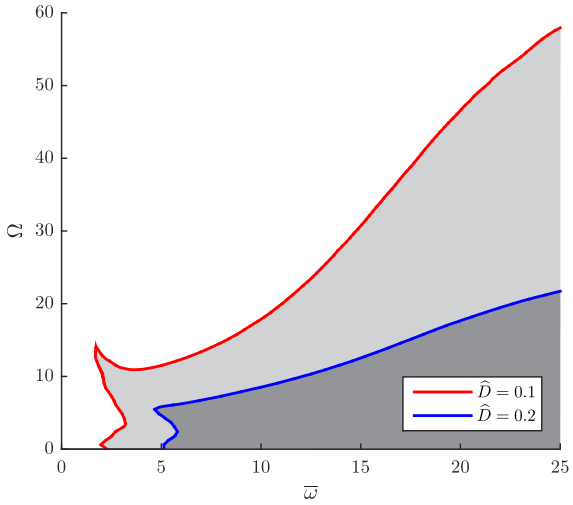

Figure 6. Stability map of trivial equilibrium point for the unloaded system with $\delta_D = 0.1$, $\overline{d}_a = 0.1$, $\Gamma = 0.01$, $\eta = 0.25$, $\sigma = 1$, $f = 0$ (gray-colored: unstable regions)

4.2.2 Analysis of the loaded non-linear system

The system's dynamics with an external load ($f \neq 0$) reveals itself to be rather complicated. As already mentioned, the existence of an equilibrium point cannot be proved in general. Instead the excitation through the bearing geometry results in limit-cycles with small amplitudes at low values of the speed-parameter $\overline{\omega}$, like depicted in the run-up simulation in figure 7 for $\overline{\omega} = 3$. The oscillation frequency is thereby given by the geometry variation frequency Ω.

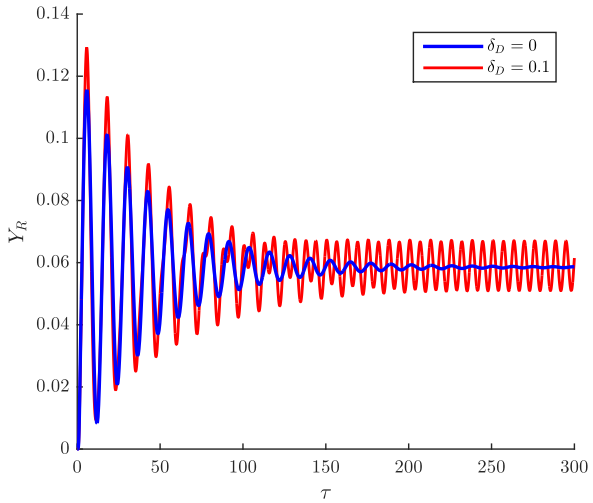

Figure 7. Vertical rotor position Y_R with and without geometry excitation at $\overline{\omega} = 3$ with $\Omega = 1$, $\widehat{D} = 0.1$, $\overline{d}_a = 0.1$, $\Gamma = 0.01$, $\eta = 0.25$, $\sigma = 1$, $f = 1$

While the system with static geometry tends towards an equilibrium point, the time-varying one evolves in a limit-cycle. The excitation of the geometry in case of the loaded rotor therefore eliminates the existence of an equilibrium point in the low rpm-range. Similar to the unloaded case in section 4.2.1 the stability of this small limit-cycle is lost at a specific value of $\overline{\omega}$ via a Neimark-Sacker-bifurcation (NS) [14], which results in a quasi-periodic trajectory. The critical value of the speed-parameter at the NS-bifurcation thereby depends on the system parameters and can be influenced e.g. by the frequency Ω and amplitude δ_D of the geometry variation. A continuation of the NS-bifurcation itself turns out to be rather time-intensive due to the complexity of the system equations. Therefore in a first step only transient simulations are performed, aiming for a reduction of the occurring amplitudes at high rpm-values. The results from the stability analysis of the unloaded system are thereby taken as first guess for an appropriate parameter-set.

A recall of figure 5 shows that large amplitudes of the rotor are reached for example at $\overline{\omega} = 25$. Introducing an excitation of the bearing geometry can lead to a significant reduction of these amplitudes as it can be seen in corresponding time simulations. In figure 8 the envelopes of the vertical rotor position for a run-up, starting from the center position of the bearing, are depicted for a static bearing geometry ($\delta_D = 0$) and a time-varying geometry ($\delta_D = 0.1$) respectively.

After the transient process oscillations occur in both cases, while for an actively varied geometry the amplitudes are comparatively small. This result is emphasized by the steady-state behavior of the system, which is given in figure 9. The red curve ($\delta_D = 0.1$) represents a quasi-periodic solution, although it seems to have a periodic character.

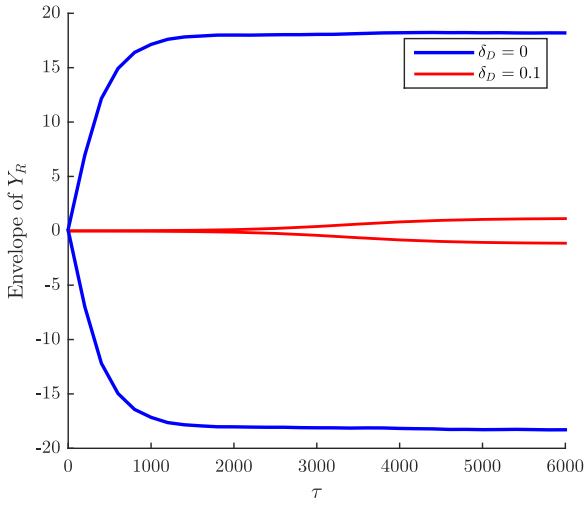

Figure 8. Envelope of vertical rotor position Y_R during run-up with and without geometry excitation at $\overline{\omega} = 25$ with $\Omega = 55$, $\widehat{D} = 0.1$, $\overline{d}_a = 0.1$, $\Gamma = 0.01$, $\eta = 0.25$, $\sigma = 1$, $f = 1$

Although the behavior for just one specific parameter-set is investigated, a qualitative effect of an amplitude reduction can be reached, like given in figure 8 and 9.

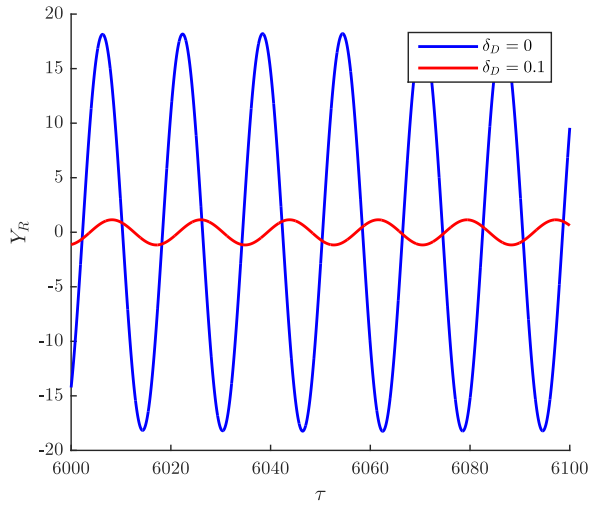

Figure 9. Vertical rotor position Y_R (steady-state) with and without geometry excitation at $\overline{\omega} = 25$ with $\Omega = 55$, $\widehat{D} = 0.1$, $\overline{d}_a = 0.1$, $\Gamma = 0.01$, $\eta = 0.25$, $\sigma = 1$, $f = 1$

Therefore it is possible to tremendously reduce the rotor's oscillation amplitudes under high rotational speeds by a systematic variation of the bearing's geometry during operation.

5. SUMMARY AND DISCUSSION

In the previous section 4 the dynamics of a Jeffcott rotor supported by two-lobe bearings with and without variation of the geometry have been investigated.
The analysis of the system with a static bearing geometry has shown a positive effect of the non-circular bearing profile. The critical value of the speed-parameter $\overline{\omega}$, at which the stability of the equilibrium point is lost, can be increased by increasing the eccentricity $\widehat{D}$ within the two-lobe bearings.
The implementation of an additional harmonic variation of the bearing's geometry during operation has been introduced. For obtaining a first approach, the unloaded Jeffcott rotor has been investigated by a linear-system analysis. Based on the results of the Floquet-multiplier investigations, a stabilizing effect of an additional geometry variation has been discovered, revealing a possibility to stabilize the equilibrium point even in high speed-ranges.
A general tendency towards higher variation frequencies Ω with increasing rotational speed has been revealed in figure 6. As the maximal occurring pressure depends also on the variation velocity (cf. section 2.2), high pressure amplitudes seem to stabilize the equilibrium position.

Introducing a geometry variation in the case of the loaded Jeffcott rotor leads to a loss of potential equilibrium positions compared to the system in static bearings, as their existence is eliminated through the additional pressure effects. Applying a variation of the bearing geometry in speed-ranges in which a stable equilibrium can be found for static geometries therefore seems not reasonable.
Nevertheless, a massive amplitude reduction for the loaded rotor in the higher "oil-whip"-speed-range has been observed by choosing an appropriate amplitude and frequency of the geometry variation for one specific parameter-set. Analytical investigations showed up to be rather complicated due to quasi-periodic trajectories.
The positive effect of a two-lobe bearing profile on the system's behavior is assumed to be caused by the two converging gaps within the journal bearing, resulting in two positive pressure ranges compared to the circular bearing profile. Creating higher pressures with the same displacement of the shaft could therefore be the reason for a better support and a stabilization effect. High geometry variation frequencies allow even higher pressure amplitudes, such that acting loads on the rotor system can be compensated without a large displacement of the journal.

For practical purposes the geometry excitation could be realized by means of piezo-actuators. Similar to the idea of Chasalevris et al., which can be found in [4], a two-lobe bearing with one vertically displaceable lobe could be set up. Instead of using a passive spring-damper mechanism, a piezo-actuator should be used, being able to control displacement amplitude and frequency.

The loaded non-linear system with an additional excitation through the bearing geometry revealed itself to be very complex due to the involvement of quasi-periodic trajectories. The work on an analytic approach to describe the observed stabilizing effect is in progress in order to validate the numerical examples of section 4.2.2.
Furthermore other bearing geometries are about to be investigated concerning their positive or negative influence on the system's performance as well as the effect of an imbalance of the rotor.

LIST OF SYMBOLS

τ	dimensionsless time
φ	circumferential coordinate
ε	small scaling parameter ($= C/r_0$)
Π	dimensionless fluid pressure
$\Pi^{\mathbf{SB}}$	dimensionless fluid pressure for short-bearing approach
Ω_φ	circumferential pressure integration range
μ	dynamic viscosity
γ	bearing geometry parameter
Γ	dimensionless shaft compliance
η	mass ratio of rotor and bearing masses
σ	modified bearing parameter
ω	angular velocity of journal
$\overline{\omega}$	dimensionless angular velocity parameter
Ω	variation frequency of eccentricity D
δ_D	relative variation amplitude of eccentricity D
A_p	integration range for positive pressures
B	axial bearing width

b_U, b_L	pressure integration boundaries of upper and lower lobe for unloaded rotor
C	characteristic bearing clearance ($= r_0 - r_W$)
c_s	linear shaft elasticity
d	vertical lobe displacment
D	dimensionless lobe displacement/eccentricity ($= d/C$)
$\widehat{D}$	mean value of lobe displacement D
$\underline{d}_a$	linear damping coefficient of rotor
$\overline{d}_a$	dimensionless damping coefficient
F_x, F_y	bearing forces
f_x, f_y	dimensionless bearing forces
$\tilde{f}_x, \tilde{f}_y$	Gauss point approximation of f_x, f_y
$f_x^{\text{lin}}, f_y^{\text{lin}}$	Linearization of f_x, f_y around trivial equilibrium position for unloaded rotor
F	vertical outer force
F_0	characteristic force
f	dimensionless vertical outer force ($= F/F_0$)
G	φ-dependent pressure part of $\Pi^{\mathbf{SB}}$
h	fluid-film-thickness
H	dimensionless fluid-film-thickness
a_i	weighting factors of Gauss quadrature
m	rotor mass
Δm	additional bearing mass
p	fluid pressure
r	bearing radius
r_0	radius of undefomed circular bearing
Δr	radial deviation from circular profile ($= r - r_0$)
r_W	journal radius
$\overline{R}$	dimensionless radial deviation from circular profile
S_m	modified Sommerfeld-number
t	time
x, y	center coordinates of journal
$x_{R/B}, y_{R/B}$	position of rotor/bearing
X, Y	dimensionless center coordinates of journal
$X_{R/B}, Y_{R/B}$	dimensionless position of rotor/bearing
z	axial coordinate
$\overline{z}$	dimensionless axial coordinate
$\underline{z}$	state-vector of Jeffcott rotor
$\underline{z}_0$	equilibrium position

REFERENCES

[1] Aydin Boyaci. *Zum Stabilitäts-und Bifurkationsverhalten hochtouriger Rotoren in Gleitlagern*, volume 15. Schriftenreihe des Instituts für Technische Mechanik, KIT Scientific Publishing, Ph.D. thesis, 2012.

[2] Ashok Kumar, R Sinhasan, and DV Singh. Performance characteristics of two-lobe hydrodynamic journal bearings. *Journal of Tribology*, 102(4):425–429, 1980.

[3] M Malik. A comparative study of some two-lobed journal bearing configurations. *ASLE TRANSACTIONS*, 26(1):118–124, 1983.

[4] Athanasios Chasalevris and Fadi Dohnal. A Journal Bearing With Variable Geometry for the Reduction of the Maximum Amplitude During Passage Through Resonance. *Journal of Vibration and Acoustics*, 134(6):061005, 2012.

[5] Andras Z Szeri. *Fluid film lubrication: theory and design*. Cambridge University Press, 2005.

[6] Gustavo G Vignolo, Daniel O Barilá, and Lidia M Quinzani. Approximate analytical solution to Reynolds equation for finite length journal bearings. *Tribology International*, 44(10):1089–1099, 2011.

[7] Short-bearing approximation for full journal bearings. *National Advisory Committee for Aeronautics; Washington, DC, United States*.

[8] Arnold Kowalewski. Newton, Cotes, Gauss, Jacobi: Vier grundlegende Abhandlungen über Interpolation und genäherte Quadratur. *Teubner, Leipzig*, 1917.

[9] Robert Gasch, Rainer Nordmann, and Herbert Pfützner. *Rotordynamik*. Springer-Verlag, 2006.

[10] Annick Dhooge, Willy Govaerts, and Yu A Kuznetsov. MATCONT: a MATLAB package for numerical bifurcation analysis of ODEs. *ACM Transactions on Mathematical Software (TOMS)*, 29(2):141–164, 2003.

[11] Alexander P Seyranian and Alexei A Mailybaev. *Multiparameter stability theory with mechanical applications*, volume 13. World Scientific, 2003.

[12] Alastair Cameron and CM Mc Ettles. *Basic lubrication theory*. E. Horwood, 1976.

[13] Toshio Yamamoto and Yukio Ishida. *Linear and nonlinear rotordynamics: A modern treatment with applications*, volume 11. John Wiley & Sons, 2001.

[14] Yuri A Kuznetsov. *Elements of applied bifurcation theory*, volume 112. Springer Science & Business Media, 2013.